

Ab initio investigations of point and complex defect structures in B2-FeAlHalil İbrahim Sözen ^{1,2} Eduardo Mendive-Tapia,^{1,3} Tilmann Hickel,^{1,4} and Jörg Neugebauer¹¹Computational Materials Design, Max-Planck-Institut für Eisenforschung GmbH, 40237 Düsseldorf, Germany²Institute of Chemistry, Carl-von-Ossietzky University of Oldenburg, D-26129 Oldenburg, Germany³Peter Grünberg Institut and Institute for Advanced Simulation, Forschungszentrum Jülich and JARA, D-52425 Jülich, Germany⁴BAM Federal Institute for Materials Research and Testing, 12489 Berlin, Germany

(Received 14 January 2021; revised 18 December 2021; accepted 4 February 2022; published 28 February 2022)

We study single-site and two-site defect structures in B2-type Fe-Al alloys by means of density functional theory supercell calculations. The defect formation energies are calculated as functions of the chemical potential, which are used to obtain the dependence of the defect concentrations on Al content at different temperatures. We also examine the converging behavior of the formation energies with respect to the supercell size to study the corresponding limit of dilute defects. The effect of magnetism is investigated by considering nonmagnetic, ferromagnetic, and paramagnetic states, calculations for the latter showing that the magnitude of the local magnetic moments strongly impacts the defect formation energies. The methodological studies are used to provide explanations for the wide spread of defect formation energies reported by experiments and other theoretical investigations. Based on these insights, the stability of the B2-FeAl structure as a function of Al concentration is obtained and discussed.

DOI: [10.1103/PhysRevMaterials.6.023603](https://doi.org/10.1103/PhysRevMaterials.6.023603)**I. INTRODUCTION**

Fe-Al alloys have been a field of interest in materials science since the 1930s. They have been promising candidates for industrial applications since it was discovered that Fe-Al alloys have high corrosion and sulfidation resistance properties [1] with composition of more than 20 at. % Al, compared with steels and Fe-based commercial alloys. It has also been realized that alloys with this composition have lower density than stainless steels [2] and have comparable tensile strength to that of ferritic and austenitic steels [3]. These properties make Fe-Al alloys attractive for the industry, where inexpensive and high-temperature structural materials are used.

However, the extensive technical applications of iron aluminides are constrained due to the low ductility at ambient temperatures and poor fracture toughness [4,5]. The thermo-mechanical properties of high-temperature intermetallics are closely related to the defect structure and their migration. Particularly comparing with other intermetallics, B2-FeAl shows a very high vacancy concentration of several percent at elevated temperatures [6–10]. Therefore the development of more ductile Fe-Al alloys and the estimation of the high-temperature mechanical behavior require that the fundamental understanding of defect formation, concentration, and migration be advanced.

Fe-Al alloys crystallize into many different lattice structures [11], especially for large concentrations of Al, but of technological interest are mainly the DO₃ (DO₃-Fe₃Al) and the B2 (B2-FeAl) crystal phases. Owing to its high melting point and wide range of stability, the B2-FeAl structure is usually the preferred phase when the interest centers on high-temperature applications. This work focuses on defect formation and corresponding finite-temperature defect concentrations of B2-FeAl.

Defect and diffusion behavior of Fe-Al alloys has been studied experimentally [2,12–16] and theoretically [17–22]. Fu *et al.* [19] performed *ab initio* calculations to investigate the binding energies of divacancy formation in stoichiometric B2-FeAl. They reported a significantly high binding energy with a value of 0.57 eV, which indicates that there is a strong tendency for vacancy clustering and that vacancies can be annealed out to create dislocations, voids, or grain boundaries. Haraguchi *et al.* [23] confirmed this with spun and annealed ribbons and fully annealed powder sample experiments. The group of Fähnle used a grand canonical approach and reported several extended studies [17,18,20,24]. One of their main results is that there are no Al vacancies in B2-FeAl, which has been confirmed by other authors.

However, there is a wide spread of reported defect formation energies in B2-FeAl. For example, there are many results of Al vacancy formation energies, changing from 1.62 eV [25] (with boron impurity) to 4.69 eV [26]. The authors of Refs. [25,26] concluded that vacancy clustering is negligible, which is in sharp contrast to the results obtained by Fu *et al.* [19] and Haraguchi *et al.* [23]. By performing density functional theory (DFT) calculations, here we show from first principles that the main reasons explaining such a wide range of defect formation energies reported in the literature (as in the

Published by the American Physical Society under the terms of the [Creative Commons Attribution 4.0 International license](https://creativecommons.org/licenses/by/4.0/). Further distribution of this work must maintain attribution to the author(s) and the published article's title, journal citation, and DOI. Open access publication funded by the Max Planck Society.

case of Al vacancy) are as follows: (i) unconverged supercells, i.e., the use of too-small supercells that are tied to large defect concentrations; (ii) lack of consideration of the formation of local magnetic moments at Fe sites, i.e., a nonmagnetic simulation; and (iii) calculations that do not take into account self-consistently the role of the chemical potential of Fe and Al. We also investigate the effect of a paramagnetic state and discuss the stabilization range of the B2-FeAl structure.

The paper is organized as follows: In Sec. II we give a brief explanation of computational details and the methodology used. In Sec. III, we describe how to calculate the considered defect formation energies. The comparison of the calculated defect concentrations against experiments is discussed in Sec. IV. We finish the paper by providing conclusions and remarks in Sec. V.

II. COMPUTATIONAL DETAILS

All first-principles calculations have been performed in the framework of spin-polarized DFT using the Vienna *ab initio* simulation package (VASP) [27,28]. We have used the projector-augmented wave (PAW) method as implemented in VASP. Exchange-correlation effects have been treated within the generalized gradient approximation (GGA) of Perdew, Burke, and Ernzerhof (PBE) [29]. As mentioned in the Introduction, the reported defect formation energies in B2-FeAl are very sensitive to the supercell size. Therefore bulk and defect simulations have been performed for 16-atom ($2 \times 2 \times 2$), 54-atom ($3 \times 3 \times 3$), and 128-atom ($4 \times 4 \times 4$) supercells. We have found that supercells containing 128 atoms are sufficiently large to obtain defect formation energies that are converged satisfactorily; see Sec. III A.

We have sampled the Brillouin zone with a k mesh described by a Monkhorst-Pack grid [30], considering $12 \times 12 \times 12$, $8 \times 8 \times 8$, and $6 \times 6 \times 6$ k meshes for supercells containing 16, 54, and 128 atoms, respectively. The cutoff energy for the plane-wave basis used was 420 eV, and the width of the smearing parameter was 0.15 eV. Eight and three valence electrons were taken into account for Fe and Al, respectively. The values of all these input parameters provide an energy convergence with an error equal to or smaller than 1 meV/atom.

The formation of local magnetic moments and their orientational ordering affect the defect formation energies, especially for the Al vacancy defect formation energy (a detailed explanation is given in Sec. III). Similarly, the presence of point defects such as Fe antisite, which is the dominant one in the Fe-rich region, as will be shown later, leads to positional-dependent magnetic moment magnitudes in the vicinity of the defect [31]. We firstly study this effect by considering a ferromagnetic (FM) order for the local moments at the Fe sites and comparing our results with those obtained in a nonmagnetic case.

Experiments [32] have shown, however, that the magnetic configuration in B2-FeAl can be paramagnetic at temperatures as low as 1 K. It can also be nonmagnetic or a spin-glass state depending on the chemical composition. Albeit conventional density functional theory using both the local density approximation (LDA) and GGA yields the ferromagnetic state as the ground state of B2 FeAl, the low Curie temperature

for Al-rich compositions calls for an additional consideration of a paramagnetic state. In addition, Mohn *et al.* [33] have reported that the paramagnetic state becomes more stable after taking into account correlation effects within the LDA+ U framework. Furthermore, Smirnov *et al.* [34] proposed that the energy differences between the ferromagnetic and paramagnetic states become almost negligible when partial long-range order is considered within the concentration range of Al that we are interested in, i.e., between 30 and 70%.

In this paper, paramagnetic results are achieved by a superposition of magnetically disordered supercells akin to the spin-space averaging (SSA) technique [35]. We assume that the local moment orientations evolve very slowly, which allows the averaging over a number of noncollinear local moment configurations within magnetically constrained DFT calculations. These calculations are also performed in VASP, using a value of the Lagrange multiplier parameter $\lambda = 50$ eV for the constraint, a cutoff energy of 500 eV, and supercells containing 128 atoms with local moment orientations at the Fe sites that are fully random. We consider two different scenarios regarding the local moment magnitudes. In the first one [paramagnetic (PM) 1], all moment magnitudes are taken equal to values that are slightly smaller than those ones obtained in the ferromagnetic state when a lattice defect is included. In the second scenario (PM 2) we constrain the magnitudes to the value obtained in the ferromagnetic state without defects, i.e., $0.71 \mu_B$. In both scenarios, we have found that an average over ten supercell configurations, each one of them containing a different set of randomly generated local moment orientations, suffices to yield a satisfactory accuracy.

III. DEFECT FORMATION ENERGIES

In order to investigate defect properties, reliable reference energies from bulk defect-free calculations are crucially important. We therefore start by performing bulk calculations for a defect-free B2-FeAl structure for the ferromagnetic, nonmagnetic (NM), and paramagnetic (PM 2) states. The computed lattice parameter minimizing the total energy, the bulk modulus, the cohesive energy, the formation enthalpy, and the magnetic moment is obtained for the considered magnetic states and compared with experiment in Table I.

The theoretical lattice parameter and formation enthalpy are in very good agreement with the experimental measurements. The calculated bulk modulus is slightly overestimated, but the agreement is satisfactory, also taking its dependence on the defect concentration into account. Our calculations confirm that ferromagnetic order is energetically more favorable than a nonmagnetic state, consistent with the findings of other authors [39–41]. Since the values of the lattice parameter and bulk modulus do not present substantial changes with respect to the magnetic states studied, their comparison with experiment does not allow us to make further conclusions.

In B2-FeAl compounds there are four kinds of native defects: Fe vacancy, Al vacancy, Fe antisite, and Al antisite. We remark that interstitial defects are not expected, due to the size of the atoms. In order to explain the high defect concentrations and extensive solubility range in B2-FeAl, we also consider the following defect complexes with two atoms:

TABLE I. Comparison of our DFT results with experimental data [36,37] of bulk B2-FeAl in the absence of defects. The lattice parameter a and bulk modulus B have been determined by a linear regression to the Murnaghan equation of state [38]. H denotes the formation enthalpy. The magnitude of the theoretical magnetic moments computed at the Fe sites is also shown.

	a (Å)	B (GPa)	Cohesive energy (eV/atom)	H (eV/atom)	Averaged magnetic moment (μ_B /atom)
Nonmagnetic	2.870	179.7	-6.343	-0.315	0
Ferromagnetic	2.874	175.3	-6.359	-0.331	0.71
Paramagnetic	2.876	163.7		-0.322	0
Experiment [36,37]	2.86, 2.88	152		-0.33	

(i) divacancies, (ii) diantisites, and (iii) the combination of one antisite and one vacancy. All defect types considered in this paper are compiled in Fig. 1.

As listed in the Introduction, a consistent definition of reference states is important for the comparability of defect formation energies. In this paper, the chemical potential is used as the thermodynamic natural variable throughout all expressions for the defect formation energy and solution enthalpy. The chemical potentials of Fe and Al are not independent of each other, if we consider the formation of B2-FeAl, i.e.,

$$\mu_{\text{Fe}} + \mu_{\text{Al}} = H_{\text{FeAl}}^f. \quad (1)$$

Here, $H_{\text{FeAl}}^f = -0.662$ eV (-0.644 eV) is the formation enthalpy per formula unit of FM (PM) bulk B2-FeAl with respect to pure ferromagnetic bcc Fe and pure nonmagnetic fcc Al (compare with Table I). Thus only one of the chemical potentials is an independent variable, which will change the defect formation energies and the resulting composition of the B2 phase.

In this paper, μ_{Al} has been chosen as the independent chemical potential, and we plot the defect formation energies with respect to μ_{Al} . It still cannot be arbitrarily changed, since the condition

$$H_{\text{FeAl}}^f < \mu_{\text{Al}} < 0 \quad (2)$$

has to be fulfilled to ensure the stability of the system. By definition, $\mu_{\text{Al}} = 0$ corresponds to a chemical equilibrium with bulk Al, i.e., it defines a critical defect solubility in the B2 phase and the onset of a phase separation into B2-FeAl and fcc Al. On the other hand, $\mu_{\text{Al}} = H_{\text{FeAl}}^f$ implies $\mu_{\text{Fe}} = 0$, i.e., a chemical equilibrium with pure Fe. We note that the lower value of μ_{Al} depends on the question of whether pure Fe is assumed to form in the FM or PM state, of which the former is chosen here. The solubility range is further reduced as soon as a thermodynamic equilibrium with other phases such as Fe_3Al , Al_2Fe , or Al_5Fe_2 is achieved, which are, however, not taken into account in this paper.

A. Single-defect formation energies

The formation of a defect costs energy, which can be calculated within DFT. The formation energy of an A vacancy in an AB compound is given by

$$E_{\text{vac},A}^f = E(A_{N-1}B_N) + \mu_A - NE(AB), \quad (3)$$

where A stands for either Fe or Al and N is the number of B2 formula units of energy $E(AB)$. $E(A_{N-1}B_N)$ is the energy of a supercell, in which an A atom has been removed from N B2 unit cells. μ_A is the chemical potential of the A species in the B2 phase, i.e., fulfilling Eqs. (1) and (2). Similarly, the A antisite formation energy can be defined as

$$E_{\text{AS},A}^f = E(A_{N+1}B_{N-1}) + \mu_B - NE(AB) - \mu_A, \quad (4)$$

where $E(A_{N+1}B_{N-1})$ is the energy of a $2N$ -atom supercell in which one B atom is replaced by an A atom, i.e., an A antisite atom.

The definition of the formation energies given above contains the size of the supercell studied. However, the results do not depend on N if defect-defect interactions emerging from periodic boundary conditions become negligible. Thus we carefully study the convergence with respect to supercell size. To this end, we perform a set of simulations for supercells of increasing size containing 16, 54, and 128 atoms. In each of these supercells only one defect is considered, which corresponds to defect concentrations of 6.25, 1.85, and 0.78%, respectively.

As shown in Fig. 2, the lattice constant and the bulk modulus significantly depend on the supercell size of 16 and 128 atoms, respectively. The lattice constants obtained for the smaller, 16-atom supercells are underestimated in comparison to the ones computed in 128-atom supercells, except for calculations containing a single Al antisite. This can be understood by noticing that the defect concentration is larger

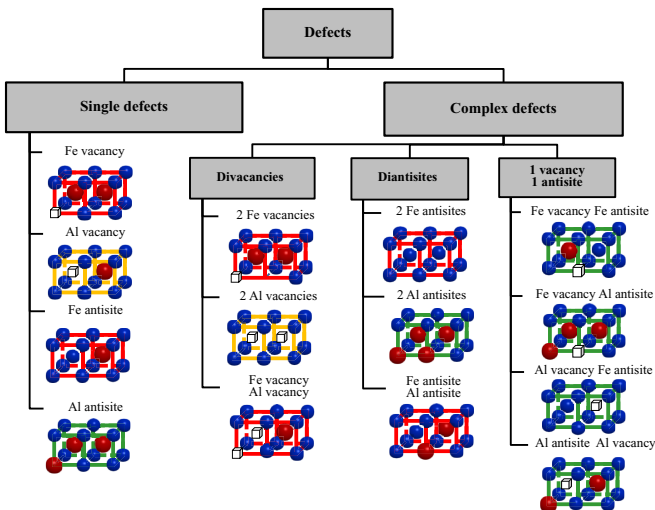


FIG. 1. Compilation of the single-site and complex, two-site, defects considered in our theoretical investigations of B2-FeAl. For each defect, two unit cells are schematically displayed, while the remaining supercell of perfect B2-FeAl is not shown.

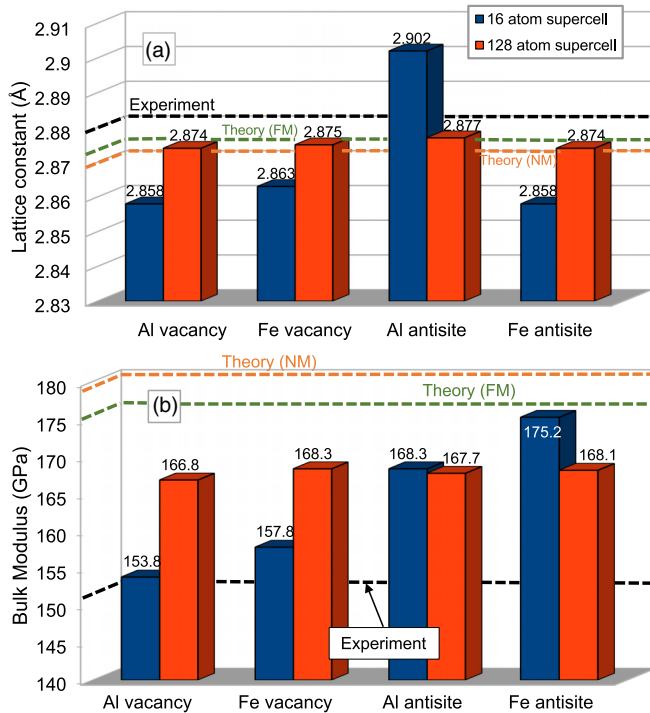


FIG. 2. *Ab initio* calculations of (a) lattice parameters and (b) bulk modulus of B2-FeAl for supercells containing 16 and 128 atoms with single-site defects. The dashed lines indicate corresponding experimental values [37] as well as theoretical results without defects.

in the smaller cells and the atomic radius of Al is larger than that of Fe. For supercell calculations containing 128 atoms, these size effects become negligible, and the lattice constants are almost the same for all the considered defects, indicating convergence.

Similarly, the bulk modulus is fairly independent of the type of defect for the supercells containing 128 atoms, though the value is still smaller than the bulk modulus of 175.3 GPa calculated for the FM defect-free supercells (see Table I). The softening becomes stronger for the larger vacancy concentrations in the 16-atom supercells. The better agreement with the experimental value of 152 GPa in this case suggests that in experiment, B2-FeAl contains a high concentration of vacancies, especially in samples away from the nonstoichiometric regime (e.g., Al content between 40 and 50 at.%).

In Fig. 3, the effect of the supercell size and of ferromagnetism on the defect formation energies is investigated. The Al vacancy formation energy changes drastically from 2.53 to 1.80 eV, i.e., by about 40%, when changing the supercell size from 16 to 128 atoms in a ferromagnetic state. This is in sharp contrast to the results obtained for other single-site defects, where this change is much smaller. It indicates that vacancy-vacancy interaction in the 16-atom supercell is particularly strong. However, in the case of 54-atom cell size the deviation from the 128-atom supercell is only 4.4%. We also performed non-spin-polarized calculations and found that the Al vacancy formation energy in this case changes by only 8.8% from 3.32 eV (16-atom case) to 3.05 eV (128-atom case). Thus the significant change in the formation energy is caused by the

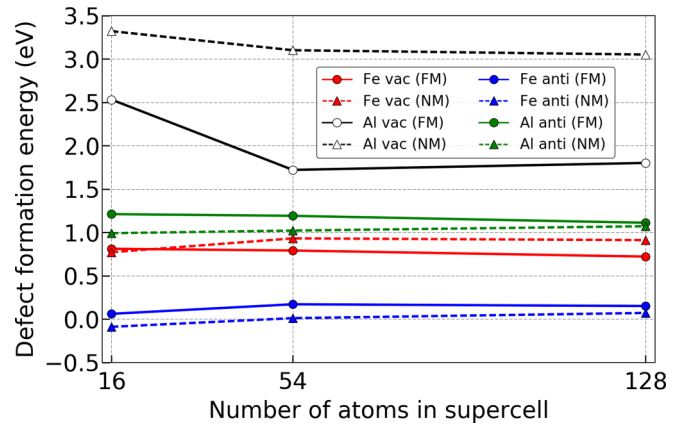


FIG. 3. *Ab initio* calculations of the single-site defect formation energies in ferromagnetic and nonmagnetic states against the size of the supercell. All of the defect formation energies are determined for Fe-rich conditions ($\mu_{\text{Fe}} = 0$). Here, anti, antisite; vac, vacancy.

ferromagnetism. The strong interaction and magnetic effects explain the large spread of Al vacancy formation energies reported in the literature.

On the other hand, the calculations including Fe vacancies do not show such large dependencies. Nevertheless, these formation energies still differ between FM (0.72 eV) and nonmagnetic (0.91 eV) supercells containing 128 atoms. In the case of single-antisite defects, the Al antisite calculations for both ferromagnetic and non-spin-polarized states show a very small dependence on the size of the supercell. In addition, ferromagnetic and non-spin-polarized Fe antisite calculations only show defect-defect interactions for the 16-atom supercell, while, e.g., for the spin-polarized calculations the defect formation energy is almost the same for the 54-atom supercell (0.17 eV) as for the 128-atom supercell (0.15 eV).

As discussed above, B2-FeAl has a Curie temperature that is very close to 0 K or even remains paramagnetic, depending on the chemical concentration. Nevertheless, experiments have shown that an Fe antisite defect, which forms a cluster of Fe atoms, as well as an Al vacancy, can exhibit an effective magnetic moment [31,32,42]. Bester *et al.* [43] also stated that inclusion of the spin polarization of Fe atoms supports the formation of Fe antisite defects, because of the gain of interatomic exchange energy. Such an interplay of defects and local magnetic moments is also important for the choice of the paramagnetic state (PM 1). In order to investigate this effect efficiently, the individual magnetic moment of each atom is determined by a Bader analysis [44] in the ferromagnetic state.

Although the element Al is nonmagnetic, it experiences an induced, antiparallel, magnetic moment (of magnitude $-0.17 \mu_B$ to $-0.24 \mu_B$) due to the presence of ferromagnetically ordered Fe atoms.

The dependence of the magnetic moments of the Fe atoms on the distance between the respective atom and the defect position in a 16- and a 128-atom supercell (Fig. 4) is shown in Fig. 5. In the 16-atom supercell, all the Fe atoms are nearest neighbors (NNs) of the Al vacancy and have magnetic moments of $1.2 \mu_B$, respectively. In the 128-atom supercell the sizes of the magnetic moments after relaxation are $1.75 \mu_B$,

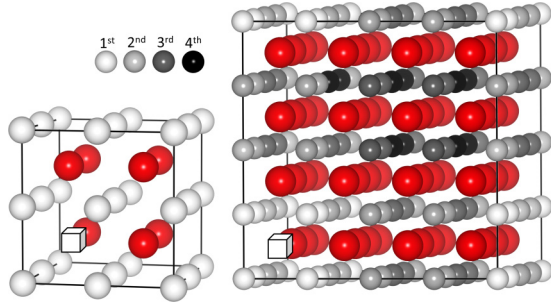


FIG. 4. Representation of 16-atom (left) and 128-atom (right) supercells with an Al vacancy. The Al vacancy is symbolized by the white box, and Al atoms are represented by red spheres. Fe atoms are shown as spheres shaded from white to gray to black according to their distance from the defect.

0.32 μ_B , 0.86 μ_B , and 0.69 μ_B within the first, second, third, and fourth shells, respectively, i.e., they show a Friedel-like oscillatory behavior. The magnetic moments of the eight Fe atoms in the NN shell of the Al vacancy (1.75 μ_B) are in this case closer to the value obtained for a perfect bcc Fe calculation (2.20 μ_B , orange line in Fig. 5) than to corresponding moments in B2-FeAl without defects (0.71 μ_B , blue line). Instead, for the fourth shell we have found smaller magnetic moment magnitudes of 0.69 μ_B that are close to the value for a B2-FeAl calculation without defects. The latter indicates that the selection of a 128-atom supercell is magnetically converged with respect to the magnetic moment sizes of atoms away from the vacancy.

The single-site defect formation energies are calculated according to Eqs. (3) and (4) and plotted in Fig. 6. It is found that among the different point defects for all studied magnetic states the highest formation energy belongs to the Al vacancy, even in Fe-rich conditions ($\mu_{\text{Fe}} = 0$) where it is 1.79 eV in the FM state. This explains the consistent reports in the literature about very small Al vacancy concentrations [18]. It further indicates that the strong interaction effects observed for Al vacancies will have no implications for the upcoming results.

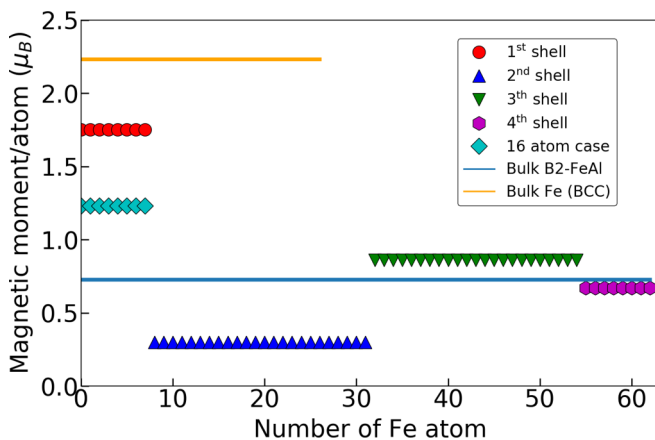


FIG. 5. Calculated magnitudes of the magnetic moments forming at Fe sites in 16- and 128-atom supercells with one Al vacancy. Both corresponding crystal structures are shown in Fig. 4.

For Fe-rich conditions the dominant single-site defect is the Fe antisite with a formation energy of 0.14 eV, which is a consequence of the chemical driving force. This dominance covers the region from $\mu_{\text{Al}} = -0.67$ eV to the vertical blue line in Fig. 6, where $\mu_{\text{Al}} \approx -0.48$ eV. Similarly, for Al-rich conditions the dominant defect is the Al antisite. However, the defect formation energy has a negative value above $\mu_{\text{Al}} \approx -0.12$ eV. Therefore, for larger values of μ_{Al} , the B2 crystal structure becomes unstable due to a drastic increase in the number of Al antisites, and the solubility range of Eq. (2) needs to be adapted accordingly. For intermediate values of the chemical potential, -0.48 eV $< \mu_{\text{Al}} < -0.29$ eV between the blue and red vertical lines, the dominant defect is the Fe vacancy, while the Al antisite dominates for -0.29 eV $< \mu_{\text{Al}} < -0.12$ eV, between the red and green vertical lines.

If the local moments of the Fe atoms are paramagnetically disordered with magnitudes similar to the ones obtained in the defective FM state (PM 1), the range of μ_{Al} in which the B2-FeAl phase is stable does not change substantially. For example, on the Al-rich side the Al antisite defect formation energies in both the FM and PM 1 states are nearly identical. The behavior is similar on the Fe-rich side for the Fe antisite defect formation energy. On the other hand, when we constrain the local moment magnitudes to values close to 0.71 μ_B (PM 2), all the defect formation energies strongly increase. We have found that these high energy values lead to an unrealistic situation, in which no defects are formed. It can be therefore concluded that the local change in the magnetic moment magnitudes is important.

B. Complex defect formation energies

The second defect group contains the complex, two-site, defects listed in Fig. 1. The formation energy of an *A*-type divacancy and diantisite in an *AB* compound can be given by

$$E_{2\text{vac},A}^f = E(A_{N-2}B_N) + 2\mu_A - NE(AB), \quad (5)$$

$$E_{2\text{AS},A}^f = E(A_{N+2}B_{N-2}) + 2\mu_B - NE(AB) - 2\mu_A, \quad (6)$$

where $E(A_{N-2}B_N)$ is the energy of a supercell containing $N - 2$ atoms of type *A* and N atoms of type *B*, i.e., two vacancies in the *A* sublattice in neighboring unit cells. $E(A_{N+2}B_{N-2})$ is the energy of the supercell where two *B* atoms are replaced by *A* atoms, i.e., two neighboring antisites.

The abovementioned groups can also involve both sublattices of B2-FeAl, e.g., one *A* vacancy and one *B* vacancy or one *A* antisite and one *B* antisite. The corresponding defect formation energies can be formulated as

$$E_{1\text{vac},A,B}^f = E(A_{N-1}B_{N-1}) + \mu_A + \mu_B - NE(AB), \quad (7)$$

$$E_{1\text{AS},A,B}^f = E(A_NB_N)_{\text{AS}} - NE(AB), \quad (8)$$

where the first term on the right denotes again the energy of the defect cell, respectively.

The last class of complex defects that we consider (Fig. 1) involves simultaneously one vacancy and one antisite, which consists of four possible defects. Two of them involve one sublattice only, e.g., one *A* vacancy together with one *A* antisite. The other two involve both sublattices: one *A* antisite together with one *B* vacancy, and one *B* antisite together with

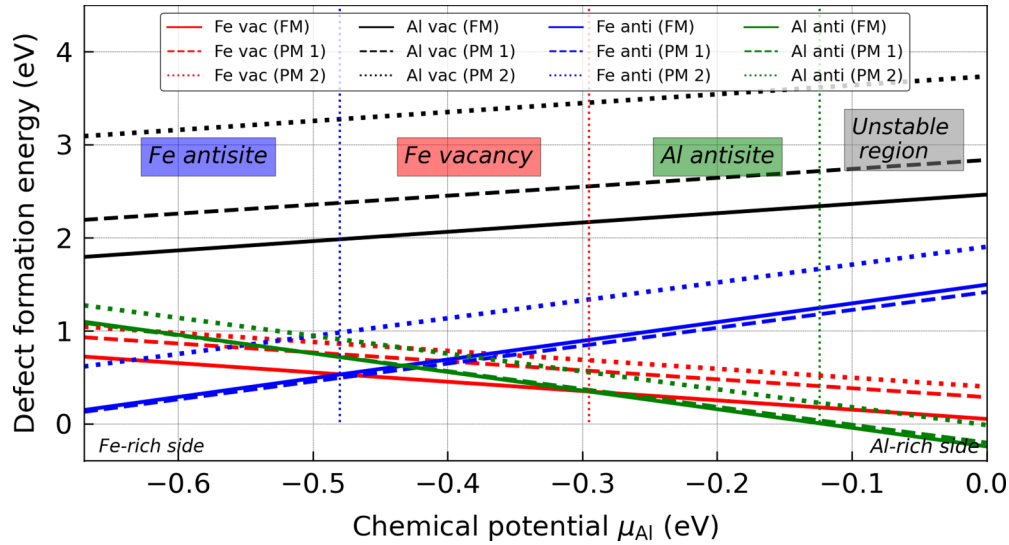


FIG. 6. Calculated single-site defect formation energies and their dependence on μ_{Al} for the ferromagnetic and paramagnetic state in 128-atom supercells. In the paramagnetic states PM 1 (PM 2) the disordered local magnetic moments at the Fe sites have magnitudes that are slightly smaller than those obtained in the FM state with (without) corresponding defects (cf. Sec. II). The left-hand (right-hand) sides of the plot correspond to Fe-rich (Al-rich) conditions, respectively. Vertical lines separate the different dominant defect regions based on the FM calculations.

one A vacancy. This can also yield complex combinations of chemical potentials as in

$$E_{1AS,A,1vac,B}^f = E(A_{N+1}B_{N-2}) + 2\mu_B - NE(AB) - \mu_A, \quad (9)$$

where $E(A_{N+1}B_{N-2})$ is the energy of a structure that includes one A antisite and one B vacancy.

Consideration of complex defects has a significant impact on the stability range of B2-FeAl and the dependence of the

dominant defect type on the chemical potential. In comparison to Fig. 6, Fig. 7 shows that the dominant defect, in Fe-rich conditions, is the double Fe antisite with a small and positive value between $\mu_{Al} = -0.67$ and $\mu_{Al} \approx -0.61$. The single Fe antisite is the energetically most favorable defect now only between $\mu_{Al} \approx -0.61$ eV and $\mu_{Al} \approx -0.48$ eV. Addition of complex defects has not changed the dominant defect type in the intermediate regions of the chemical potential,

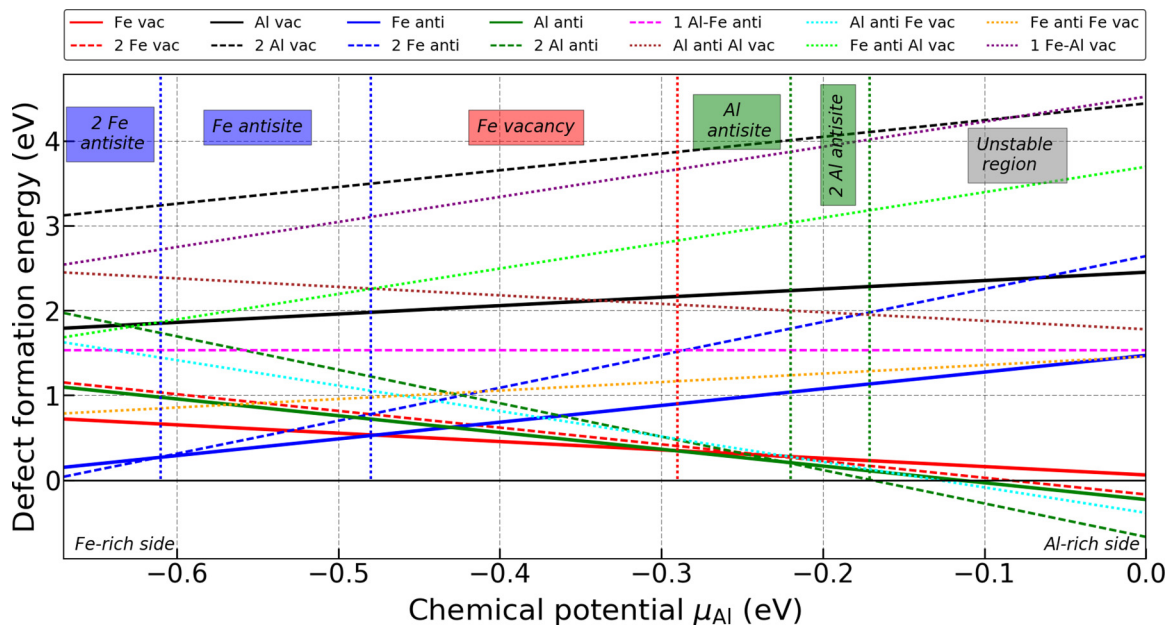


FIG. 7. Calculated formation energies of single and complex defects as functions of μ_{Al} for ferromagnetic 128-atom supercells. Single defects are given by solid lines as in Fig. 6, divacancies and diantisites are given by dashed lines, and one-vacancy–one-antisite defects are given by dotted lines. The left-hand (right-hand) side of the plot corresponds to Fe-rich (Al-rich) conditions. The vertical lines separate different dominant defect regions.

TABLE II. Defect formation energies (in eV) with respect to the referent B2-FeAl structure without defects calculated in the Fe-rich ($\mu_{Fe} = 0$) and Al-rich ($\mu_{Al} = 0$) conditions.

Defect type	Fe-rich condition	Al-rich condition
Fe vacancy	0.72	0.06
2 Fe vacancy	1.15	-0.17
Al vacancy	1.79	2.45
2 Al vacancy	3.12	4.44
Fe antisite	0.15	1.47
2 Fe antisite	0.003	2.64
Al antisite	1.09	-0.23
2 Al antisite	1.97	-0.67
Al antisite Fe antisite	1.53	1.53
Al antisite Al vacancy	2.44	1.78
Al antisite Fe vacancy	1.62	-0.36
Fe antisite Al vacancy	1.68	3.66
Fe antisite Fe vacancy	0.78	1.44
Al vacancy Fe vacancy	2.54	4.52

which is the single Fe vacancy. From $\mu_{Al} \approx -0.29$ eV to $\mu_{Al} \approx -0.22$ eV the dominant defect is the single Al antisite. For larger values than $\mu_{Al} \approx -0.22$ the double Al antisite becomes the defect with the lowest formation energy. Its formation energy vanishes already for a lower value of the chemical potential ($\mu_{Al} \approx -0.17$ eV) as compared with the single Al antisite (compare also Fig. 6). Therefore the inclusion of complex defects gives rise to a reduction in the stability range of the B2-FeAl structure by approximately 0.04 eV within the chemical potential axis. All the corresponding defect formation energies can be seen in Table II in more detail.

IV. DEFECT CONCENTRATIONS

The defect investigations performed can be used to calculate quantitatively and self-consistently the defect concentrations in B2-FeAl alloys. Once the formation energies of the defects are known, it is possible to calculate the temperature dependence of the corresponding concentrations. This is not straightforward for ordered binary alloys, while for unary metals the relation is

$$\tilde{c}_{\text{def}} = \exp\left(-\frac{E_{\text{def}}^f}{k_B T}\right). \quad (10)$$

Here, \tilde{c}_{def} holds for the concentration and E_{def}^f for the formation energy of the investigated defect, k_B is the Boltzmann constant, and T is the temperature.

We apply Eq. (10) also for the complex two-site defects such as two A vacancies, for which the expression can also be written as

$$\tilde{c}_{2\text{vac},A} = \tilde{c}_{\text{vac},A} \exp\left(-\frac{E_{\text{vac},A}^f}{k_B T}\right) \exp\left(-\frac{E_{2\text{vac},A}^b}{k_B T}\right). \quad (11)$$

The presence of the first exponent alone would yield $\tilde{c}_{2\text{vac},A} < \tilde{c}_{\text{vac},A}$, but a low vacancy formation energy $E_{\text{vac},A}^f$ (depending on μ_A) and a strong vacancy binding energy $E_{2\text{vac},A}^b$ (independent of μ_A) can change this inequality. Therefore Eq. (10)

can only in the dilute limit be expected to provide reasonable results.

To quantify this limit, we consider a theory developed by Mayer *et al.* [17] that allows one to calculate the single-site defect concentrations based on a grand canonical approach for B2-FeAl. The concentrations of A vacancies $c_{\text{vac},A}$ and A antisites $c_{AS,A}$ are given in this theory by

$$c_{\text{vac},A} = \frac{e^{-E_{\text{vac},A}^f/k_B T}}{1 + e^{-E_{\text{vac},A}^f/k_B T} + e^{-E_{AS,B}^f/k_B T}}, \quad (12)$$

$$c_{AS,A} = \frac{e^{-E_{AS,A}^f/k_B T}}{1 + e^{-E_{\text{vac},B}^f/k_B T} + e^{-E_{AS,A}^f/k_B T}}, \quad (13)$$

respectively. As shown in Fig. 8, Eq. (10) gives rather similar results to those obtained using Eqs. (12) and (13), especially in the Fe-rich region between 40 and 50% Al concentration, in which we are mainly interested and for which most of the experiments have been performed. Equation (10) only deviates noticeably above 5% defect concentration. Even for higher defect concentrations, the corrections by Eqs. (12) and (13) are not significant. Therefore we use Eq. (10) in this paper.

Figures 8 and 9 visualize the calculated defect concentrations in B2-FeAl against the concentration of Al. We have chosen two different temperatures: 1000 K, where the B2 structure has the highest stability range of Al content between 22 and 50.5%, and 1450 K, which is close to the melting temperature [23].

Both of the figures confirm the general experimental trend [7,9,10,45,46] that the concentration of Fe vacancies is strongly dominant against Al vacancies in B2-FeAl and increases with increasing Al content and temperature. It has also been reported in this trend that the concentration of Fe vacancies exhibits a rather gradual increase with composition at lower Al content and more rapid increase once the composition approaches stoichiometry. The single- and double-Fe-vacancy concentrations are indeed orders of magnitude larger than the concentration of Al vacancies. Note that for intermediate chemical potentials, the single Fe vacancy has the lowest formation energy of all the defects considered (see Fig. 7). With increasing (decreasing) Al content this formation energy decreases (increases) linearly, which immediately explains the concentration behavior in Figs. 8 and 9.

The impact of the different magnetic treatments on single-defect concentrations is also given in the inset of Fig. 8. Ferromagnetic- and paramagnetic-(PM1)-treated defect concentrations yield very similar defect concentrations for the Fe-rich and the stoichiometric compositions. They also have similar solubility limits toward Fe-rich compositions of approximately 37 and 41% Al for PM1 and FM, respectively. A considerable difference appears for high Fe vacancy concentrations at high Al compositions. This can be explained by the difference in calculated Fe vacancy formation energies as given in Fig. 6. Since FM-treated B2 results in lower Fe vacancy formation energy, it yields higher vacancy concentrations compared with the PM1 treatment.

There are many available experimental works in the literature that state that Fe vacancy is the dominant defect type at the stoichiometric composition [8,10,14,46,47], which

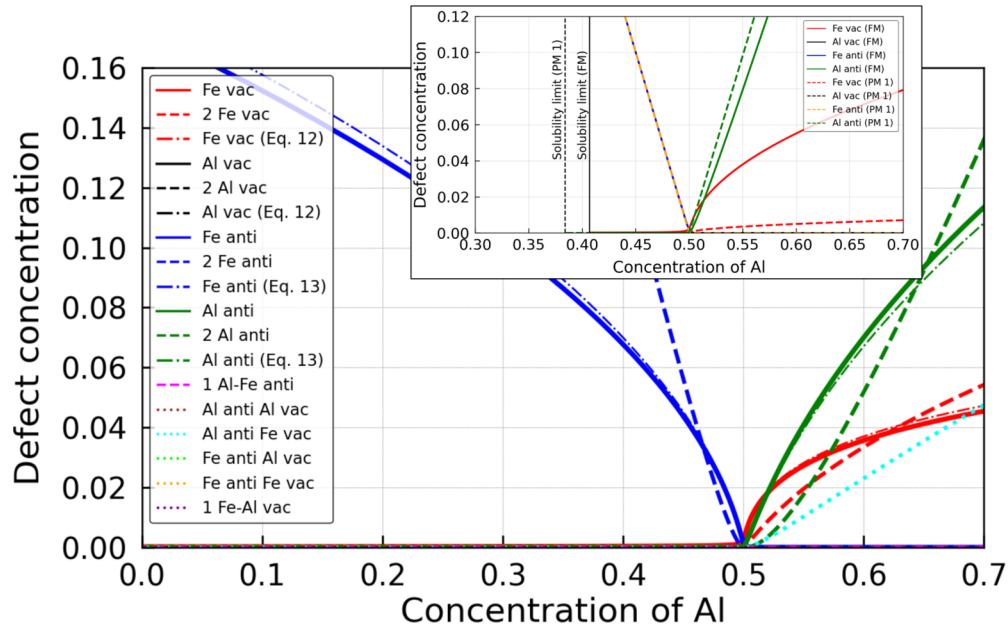


FIG. 8. Calculated concentrations of all considered defects as a function of Al concentration at 1000 K. The calculations are based on the FM defect formation energies that are given in Fig. 7. The Boltzmann statistics (solid, dashed and dotted lines) according to Eq. (10) as well as a more advanced grand canonical approach (thin dash-dotted lines) according to Eqs. (12) and (13) are used. (Divacancies and diantisites are given by dashed lines, and one-vacancy-one-antisite defects are given by dotted lines.) The inset shows a comparison of the single-defect concentrations using FM (solid lines) and PM (dashed lines) defect formation energies. The vertical lines indicate for this case the solubility limit determined by $\mu_{Fe} = 0$ for the FM and the PM 1 defect calculations, respectively. In both cases, the reference state for bcc Fe is FM. The details of the transformation from chemical potential to concentration of Al can be found in Ref. [17].

confirms our results. The dominant single-Fe-vacancy concentration is calculated to be 0.25% at 1000 K and 1.6% at 1450 K at the stoichiometric composition. Earlier, it was measured as 0.45% at 1073 K by dilatometry and high-temperature lattice constant determination [6]. Then Kogachi and Haraguchi [9] investigated the compositional dependence of vacancy concentration based on density and lattice

constant measurements in powder samples quenched at different temperatures. They reported a vacancy concentration of $\sim 2.3\%$ for water-quenched samples at 1073 K. Same authors reported a value of $\sim 3.8\%$ for samples measured at 1250 K [46] a few years later. One can conclude that our theoretical investigations underestimate the concentration of Fe vacancies.

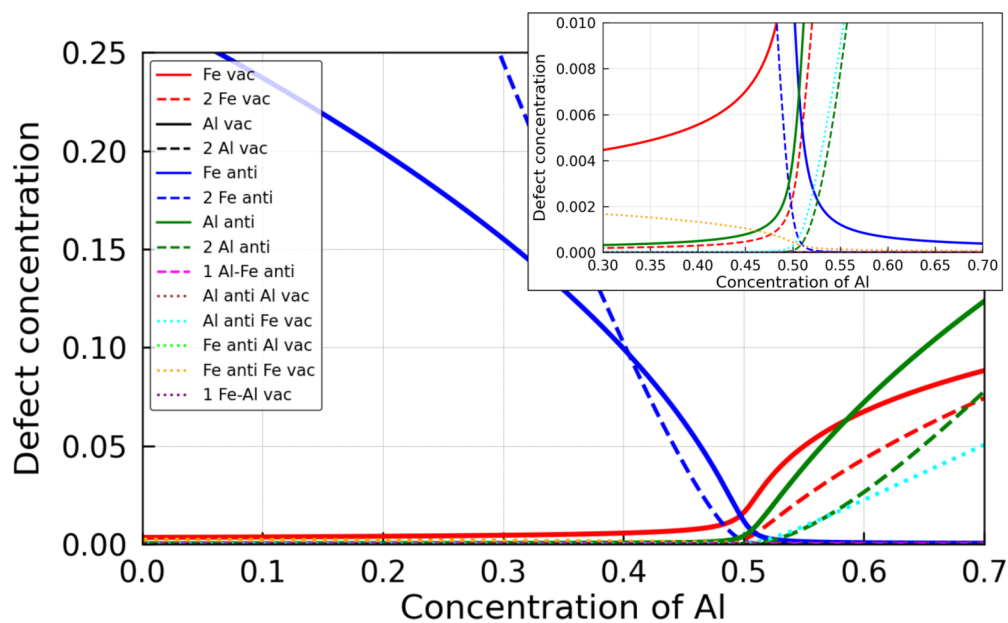


FIG. 9. Calculated concentrations of all considered defects as functions of Al concentration, similar to Fig. 8, but at 1450 K. The inset zooms into the values for low defect concentrations.

However, for a particular case, a conflict between our results and an experiment appears by comparing the Al vacancy concentration. Experimental work of Haraguchi and Kogachi [46] showed that the vacancies occur in both sublattices, but we do not observed significant values of Al vacancies in our results. This could be attributed to the absence of formation entropy in our methodology. Nevertheless, Mayer *et al.* [17] calculated a negligible concentration of Al vacancy of the order of 10^{-14} . The authors concluded that higher concentrations around 10^{-3} would require a formation entropy of $25k_B$, which is an unrealistic value. Even the addition of $5k_B$ in analogy would lead to an Al vacancy concentration of 10^{-12} . These calculations and other theoretical work reporting high defect formation energy and consequent absence of Al vacancies [17–20,24,48–50] are in agreement with our results.

We predict the Fe antisite as the dominant defect for smaller Al content below the stoichiometry. The concentration of Fe antisites increases with decreasing Al content. The fact that antisite defects are dominant for these Al concentrations can be explained by examining the partially filled bonding states of Fe-Al, therefore with the Fe antisites in the bulk, where the local Fe-Al bonding can be enhanced by *d*-band filling through *d-p* hybridization [19]. As given in Fig. 7, above $\mu_{\text{Al}} \approx -0.48$ (this value corresponds to stoichiometric conditions) the single Fe antisite has the lowest defect formation energy, which yields the highest defect concentration between the stoichiometric composition and $\sim 47\%$ Al content at 1000 K ($\sim 41\%$ Al at 1450 K). For lower values of Al content the dominant defect is the double Fe antisite. Experimentally, the corresponding concentration is reported to be $\sim 6\%$ Fe antisite at 1250 K for $\text{Fe}_{53}\text{Al}_{47}$ [46]. In our calculations we find $\sim 3.8\%$ for $T = 1000$ K and $\sim 5\%$ for $T = 1450$ K, which are in reasonable agreement with experiment.

In contrast to the results obtained for the Al antisite defects, the Fe antisite formation energy remains positive over all the values of μ_{Al} (see Fig. 7) such that in our calculations the B2 structure is stable down to Al concentrations of around 40% when single-site defects are considered only. The stability of the B2 structure down to this value of Al concentration observed in experiments [51] can therefore be caused by the presence of single-site defects, while two-site defects are necessary to explain the stabilization down to 25% of Al content also found experimentally, as shown in Fig. 8.

According to available experiments and other theoretical works [17,19,46,48], the concentration of Fe antisite defects decreases and then vanishes by increasing the content of Al, which completely agrees with our results. Above the stoichiometric composition, there is a competition for the formation of vacancy and antisite defects at the Fe sites. From stoichiometry to $\sim 52\%$ of Al content the dominant defect is the single Fe vacancy. Then for higher Al concentrations the single Al antisite becomes dominant at 1000 K. The range in which the single-Fe-vacancy defect is dominant extends until 57% of Al content at 1450 K. As shown in Fig. 7, for $\mu_{\text{Al}} < -0.17$ eV the double Al antisite has a negative defect formation energy, which means that the B2 structure is no longer stable. Qualitatively, this observation is in agreement with experiment, where it is found that B2-FeAl becomes

unstable for Al-rich and intermediate conditions [51], albeit at lower Al concentrations. Except in the region close to stoichiometry, where it is nonlinear due to the Fe vacancies, the Al antisite concentration depends on the Al content. Note that the concentration of Al antisite defects is substantial compared with the concentrations calculated for other defects within the Fe-rich region, especially at 1450 K.

V. CONCLUSIONS

We have carried out *ab initio* calculations based on density functional theory to investigate the defect structures and solubility of B2-FeAl alloys at finite temperature. Our results show that the defect formation energies substantially depend on both the size of the supercell, tied to the corresponding defect concentration, and the underlying magnetic state considered. This, together with the fact that the effect of the chemical potentials of Fe and Al has not been considered in some earlier works, can explain the diversity of defect formation energies that is found in the literature.

Albeit B2-FeAl can be paramagnetic at zero temperature or show a very small Curie point, in our defect-free calculations the ferromagnetic state appears as the most stable magnetic phase at 0 K, in agreement with other theoretical studies. The computed bulk modulus and lattice parameter are in good agreement with experiment regardless of the magnetic state considered, either ferromagnetic, nonmagnetic, or paramagnetic. On the other hand, the performed calculations for the paramagnetic state have demonstrated that the magnitudes of the magnetic moments can largely impact the defect formation energies.

The dependence of the defect formation energies on the chemical potential has been used to calculate the concentrations of single-site and two-site defects self-consistently as functions of Al concentration at different temperatures. The well-known finite-temperature Boltzmann relation for unary metals provides very similar results to those obtained applying the relations developed by Mayer *et al.* [17] describing defect statistics beyond the dilute limit, which supports the application of our approach for a large range of concentrations.

Indeed, our results are in agreement with experiment in a major part of the aspects investigated. For example, Fe vacancies are dominant at the stoichiometric composition, and their concentration is enhanced by increasing the concentration of Al. However, the magnitude of the concentration computed is somewhat smaller than the experimental one. There is a critical value of Al content above which Al antisites are dominant. By raising the temperature we observe an increment of the concentration of Fe vacancies that is increasingly larger for higher concentrations of Al. This directly causes Fe vacancies to become more predominant close to stoichiometry and a consequent enhancement of the critical value of Al content. A negligible concentration of Al vacancies, consequent of their high formation energy and as also found in other theoretical studies, represents the most important disagreement between our calculations and experiments regarding defect concentration.

Complex defects causing low or high concentrations of Al are naturally favored away from stoichiometry. Pairs of Fe and pairs of Al antisites show the highest concentration

values at the low and high limits of Al content at 1000 K, respectively. Our calculations also indicate the presence of Al antisites next to Fe vacancies for Al-rich compositions. Interestingly, raising the temperature up to 1450 K reduces the relative concentration of complex defects as the critical Al concentration that corresponds to the chemical potential of equal defect formation energies (vertical lines in Fig. 7) is shifted away from stoichiometry.

Our calculations demonstrate that the stability of the B2-FeAl phase down to Al concentrations of about 40% can be caused by single-site defects, whereas the experimentally observed extensions of the solubility range down to 25% can only be explained if two-site defects are also taken into account. We have also found that the formation of defects would give rise to a solubility range of the B2-FeAl phase for Al concentrations well above the stoichiometric composition of the B2 structure, both with single-site defects and with two-site defects. In these calculations, the maximum chemical potential of Al is, however, only determined by the formation of pure fcc Al or the earlier divergence of Al

antisite concentrations. The competition and coexistence with other crystal structures, in particular, FeAl₂, substantially restrict the allowed range of Al chemical potentials that stabilize the B2-FeAl phase and explain the experimental findings of limited B2 stability above stoichiometry.

Our work lays out the groundwork for a future investigation of the kinetics and diffusion mechanism of defects. At present, there is still not generally accepted agreement regarding the mechanisms governing the diffusion behavior in B2-FeAl, establishing such a theoretical study as a very important and fundamental research line.

ACKNOWLEDGMENTS

The authors acknowledge computing time granted on the supercomputer of the Department of Computational Materials Design, operated by the Max Planck Computing and Data Facility in Garching, Germany. Early stages of this paper were supported by N. Sandschneider. Financial support by the Deutsche Forschungsgemeinschaft (DFG) through project T07 within SFB761 “steel ab initio” is acknowledged.

-
- [1] P. F. Tortorelli and J. H. DeVan, Behavior of iron aluminides in oxidizing and oxidizing/sulfidizing environments, *Mater. Sci. Eng. A* **153**, 573 (1992).
- [2] J. L. Jordan and S. C. Deevi, Vacancy formation and effects in FeAl, *Intermetallics* **11**, 507 (2003).
- [3] H. Xiao and I. Baker, The relationship between point defects and mechanical properties in Fe-Al at room temperature, *Acta Metall. Mater.* **43**, 391 (1995).
- [4] S. C. Deevi and V. K. Sikka, Nickel and iron aluminides: an overview on properties, processing, and applications, *Intermetallics* **4**, 357 (1996).
- [5] C. T. Liu, Recent advances in ordered intermetallics, *Mater. Chem. Phys.* **42**, 77 (1995).
- [6] K. Ho and R. A. Dodd, Point defects in FeAl, *Scr. Metall.* **12**, 1055 (1978).
- [7] Y. A. Chang, L. M. Pike, C. T. Liu, A. R. Billbrey, and D. S. Stone, Correlation of the hardness and vacancy concentration in FeAl, *Intermetallics* **1**, 107 (1993).
- [8] T. Haraguchi, K. Yoshimi, H. Kato, S. Hanada, and A. Inoue, Determination of density and vacancy concentration in rapidly solidified FeAl ribbons, *Intermetallics* **11**, 707 (2003).
- [9] M. Kogachi and T. Haraguchi, Quenched-in vacancies in B2-structured intermetallic compound FeAl, *Mater. Sci. Eng. A* **230**, 124 (1997).
- [10] M. Kogachi, T. Haraguchi, and S. M. Kim, Point defect behavior in high temperature region in the B2-type intermetallic compound FeAl, *Intermetallics* **6**, 499 (1998).
- [11] B. Sundman, I. Ohnuma, N. Dupin, U. R. Kattner, and S. G. Fries, An assessment of the entire Al-Fe system including D0₃ ordering, *Acta Mater.* **57**, 2896 (2009).
- [12] R. Kerl, J. Wolff, and Th. Hehenkamp, Equilibrium vacancy concentrations in FeAl and FeSi investigated with an absolute technique, *Intermetallics* **7**, 301 (1999).
- [13] J. Wolff, M. Franz, A. Broska, R. Kerl, M. Weinhagen, and B. Ko, Point defects and their properties in FeAl and FeSi alloys, *Intermetallics* **7**, 289 (1999).
- [14] A. Hanc, J. Kansy, G. Dercz, and I. Jendrzewska, Point defect structure in B2-ordered Fe-Al alloys, *J. Alloys Compd.* **480**, 84 (2009).
- [15] R. Nakamura, Y. Yamazaki, and Y. Iijima, Interdiffusion in B2 type intermetallic compound FeAl under high pressures, *Mater. Trans.* **44**, 78 (2003).
- [16] M. Eggersmann and H. Mehrer, Diffusion in intermetallic phases of the Fe-Al system, *Philos. Mag. A* **80**, 1219 (2000).
- [17] J. Mayer, C. Elsasser, and M. Fähnle, Concentrations of atomic defects in B2-Fe_xAl_{1-x}, *Phys. Status Solidi B* **191**, 283 (1995).
- [18] M. Fähnle, J. Mayer, and B. Meyer, Theory of atomic defects and diffusion in ordered compounds, and application to B2-FeAl, *Intermetallics* **7**, 315 (1999).
- [19] C. L. Fu, Y. Y. Ye, and M. H. Yoo, Equilibrium point defects in intermetallics with B2 Structure: NiAl and FeAl, *Phys. Rev. B* **48**, 6712 (1993).
- [20] R. Drautz and M. Fähnle, The six-jump diffusion cycle in B2 compounds, *Acta Mater.* **47**, 2437 (1999).
- [21] A. Kellou, T. Grosdidier, and H. Aourag, Comparative behavior of vacancy and C, B, N, O atoms single defect on hardening the B2-FeAl structure: An atomistic study, *Intermetallics* **14**, 142 (2006).
- [22] H. Amara, C. C. Fu, F. Soisson, and P. Maugis, Aluminum and vacancies in α -iron: Dissolution, diffusion, and clustering, *Phys. Rev. B* **81**, 174101 (2010).
- [23] T. Haraguchi, K. Yoshimi, M. H. Yoo, H. Kato, S. Hanada, and A. Inoue, Vacancy clustering and relaxation behavior in rapidly solidified B2 FeAl ribbons, *Acta Mater.* **53**, 3751 (2005).
- [24] J. Mayer and M. Fähnle, On the meaning of effective formation energies, entropies and volumes for atomic defects in ordered compounds, *Acta Mater.* **45**, 2207 (1997).
- [25] R. Besson, A. Legris, and J. Morillo, Influence of complex point defects in ordered alloys: An *ab initio* study of B2 Fe-Al-B, *Phys. Rev. B* **74**, 094103 (2006).
- [26] A. Kellou, H. I. Feraoun, T. Grosdidier, C. Coddet, and H. Aourag, Energetics and electronic properties of vacancies,

- anti-sites, and atomic defects (B, C, and N) in B2-FeAl alloys, *Acta Mater.* **52**, 3263 (2004).
- [27] G. Kresse and J. Furthmüller, Efficiency of ab-initio total energy calculations for metals and semiconductors using a plane-wave basis set, *Comput. Mater. Sci.* **6**, 15 (1996).
- [28] G. Kresse and J. Furthmüller, Efficient iterative schemes for *ab initio* total-energy calculations using a plane-wave basis set, *Phys. Rev. B* **54**, 11169 (1996).
- [29] J. P. Perdew, K. Burke, and M. Ernzerhof, Generalized Gradient Approximation Made Simple, *Phys. Rev. Lett.* **77**, 3865 (1996).
- [30] H. J. Monkhorst and J. D. Pack, Special points for Brillouin-zone integrations, *Phys. Rev. B* **13**, 5188 (1976).
- [31] S. Zaroual, O. Sassi, J. Aride, J. Bernardini, and G. Moya, Magnetic and calorimetric study of point defects in FeAl intermetallic compound, *Mater. Sci. Eng. A* **279**, 282 (2000).
- [32] G. R. Caskey, J. M. Franz, and D. J. Sellmyer, Electronic and magnetic states in metallic compounds—II: Electron transport and magnetic susceptibility in NiAl and FeAl, *J. Phys. Chem. Solids* **34**, 1179 (1973).
- [33] P. Mohn, C. Persson, P. Blaha, K. Schwarz, P. Novák, and H. Eschrig, Correlation Induced Paramagnetic Ground State in FeAl, *Phys. Rev. Lett.* **87**, 196401 (2001).
- [34] A. Smirnov, W. Shelton, and D. Johnson, Importance of thermal disorder on the properties of alloys: Origin of paramagnetism and structural anomalies in bcc-based $\text{Fe}_{1-x}\text{Al}_x$, *Phys. Rev. B* **71**, 064408 (2005).
- [35] F. Körmann, A. Dick, B. Grabowski, T. Hickel, and J. Neugebauer, Atomic forces at finite magnetic temperatures: Phonons in paramagnetic iron, *Phys. Rev. B* **85**, 125104 (2012).
- [36] F. R. de Boer, W. C. M. Mattens, R. Boom, A. R. Miedema, and A. K. Niessen, *Cohesion in Metals: Transition Metal Alloys* (North-Holland, Amsterdam, 1988).
- [37] P. Villars and L. D. Calvert, *Pearson's Handbook of Crystallographic Data for Intermetallic Phases* (American Society for Metals, Metal Park, OH, 1988).
- [38] F. D. Murnaghan, The compressibility of media under extreme pressures, *Proc. Natl. Acad. Sci. USA* **30**, 244 (1944).
- [39] P. G. Gonzales-Ormeño, H. M. Petrilli, and C. G. Schön, *Ab-initio* calculations of the formation energies of BCC-based superlattices in the Fe-Al system, *Calphad* **26**, 573 (2002).
- [40] N. I. Kulikov, A. V. Postnikov, G. Borstel, and J. Braun, Onset of magnetism in B2 transition-metal aluminides, *Phys. Rev. B* **59**, 6824 (1999).
- [41] R. Das, G. P. Das, and S. K. Srivastava, Electronic structure and local magnetism of 3d-5d impurity substituted CeFe_2 , *J. Phys. D: Appl. Phys.* **49**, 165004 (2016).
- [42] H. Domke and L. K. Thomas, Vacancies and magnetic properties of FeAl-alloys, *J. Magn. Magn. Mater.* **45**, 305 (1984).
- [43] G. Bester, B. Meyer, and M. Fa, Dominant thermal defects in B2-FeAl, *Mater. Sci. Eng. A* **323**, 487 (2002).
- [44] G. Henkelman, A. Arnaldsson, and H. Jónsson, A fast and robust algorithm for Bader decomposition of charge density, *Comput. Mater. Sci.* **36**, 354 (2006).
- [45] L. M. Pike, The effects of ternary alloying on the defect structure and mechanical properties of B2 compounds, Ph.D. thesis, University of Wisconsin-Madison, 1998.
- [46] T. Haraguchi and M. Kogachi, Point defect behavior in B2-type intermetallic compounds, *Mater. Sci. Eng. A* **329**, 402 (2002).
- [47] A. Hanc and J. E. Frąckowiak, Defect structure of Fe-Al and Fe-Al-X (X = Ni; Cu; Cr) metallic powders obtained by the self-decomposition method, *Nukleonika* **49** (Suppl. 3), S7 (2004), <https://yadda.icm.edu.pl/baztech/element/bwmeta1.element.baztech-article-BUJ6-0006-0003>.
- [48] R. Besson and J. Morillo, Development of a semiempirical n-body noncentral potential for Fe-Al alloys, *Phys. Rev. B* **55**, 193 (1997).
- [49] Y. Ouyang, X. Tong, C. Li, H. Chen, X. Tao, T. Hickel, and Y. Du, Thermodynamic and physical properties of FeAl and Fe_3Al : An atomistic study by EAM simulation, *Phys. B (Amsterdam)* **407**, 4530 (2012).
- [50] M. Gallouze, A. Kellou, D. Hamoutene, T. Grosdidier, and M. Drir, Absorption and adsorption of hydrogen in B2-FeAl: *Ab initio* study, *Phys. B (Amsterdam)* **416**, 1 (2013).
- [51] F. Stein and M. Palm, Re-determination of transition temperatures in the Fe-Al system by differential thermal analysis, *Int. J. Mater. Res.* **98**, 580 (2007).